

SYNTHETIC BIOLOGY

Multidimensional control of therapeutic human cell function with synthetic gene circuits

Hui-Shan Li^{1,2,†}, Divya V. Israni^{1,2,†}, Keith A. Gagnon^{1,2}, Kok Ann Gan^{1,3}, Michael H. Raymond^{1,2}, Jeffrey D. Sander^{4,5,6}, Kole T. Roybal^{7,8,9,10}, J. Keith Joung^{4,5}, Wilson W. Wong^{1,2}, Ahmad S. Khalil^{1,2,3,11*}

Synthetic gene circuits that precisely control human cell function could expand the capabilities of gene- and cell-based therapies. However, platforms for developing circuits in primary human cells that drive robust functional changes *in vivo* and have compositions suitable for clinical use are lacking. Here, we developed synthetic zinc finger transcription regulators (synZiFTRs), which are compact and based largely on human-derived proteins. As a proof of principle, we engineered gene switches and circuits that allow precise, user-defined control over therapeutically relevant genes in primary T cells using orthogonal, US Food and Drug Administration–approved small-molecule inducers. Our circuits can instruct T cells to sequentially activate multiple cellular programs such as proliferation and antitumor activity to drive synergistic therapeutic responses. This platform should accelerate the development and clinical translation of synthetic gene circuits in diverse human cell types and contexts.

Cells use networks of interacting molecules to integrate and process signals into appropriate output responses. Synthetic biology aims to manipulate this process and drive the development of new biomedical technologies and therapies (1–3). For example, programming human cells with synthetic circuits that allow them to execute desired cellular functions in response to defined stimuli could enable new capabilities for gene- and cell-based therapies. One prominent example is chimeric antigen receptor (CAR) T cell immunotherapy, in which patient-derived T cells are redirected to attack tumors by genetically modifying them to express artificial antigen-targeting receptors. CAR-T cell therapy has shown clinical promise in treating certain cancers, leading to several approved cancer therapies (4). However, engineered T cells also display adverse, sometimes fatal side effects stemming from off-target toxicity and overactivation (4–6). Moreover, CAR-T cells have substantially limited clinical efficacy for most solid tumors (7), and the corresponding

push to create more potent therapies has simultaneously heightened the risk of severe adverse side effects (8, 9).

The challenge of balancing efficacy and toxicity to realize the full potential of these emerging therapeutic modalities has motivated recent efforts in mammalian synthetic biology aimed at developing methods for precise, temporal, and context-specific control of therapeutic cellular activity (10–14). Unfortunately, developing even simple synthetic circuits in primary human cells is challenging, particularly circuits capable of the strong outputs necessary to drive functional changes *in vivo*. Those that do exist harbor molecular components or formulations that are not suitable for clinical use. Therefore, existing methods are unlikely to scale to allow control over the different aspects of cell behavior such as localization, antitumor activity, and persistence, which collectively influence and dictate therapeutic outcomes (15–20). Overall, we lack versatile, scalable, and clinically viable gene circuit engineering platforms with which to reliably engineer relevant human cell types to address therapeutic challenges.

An established method for controlling mammalian cell behavior is by engineering transcriptional regulation. Efforts to control gene expression have primarily focused on a widely used set of artificial transcriptional regulators derived from microbial transcription factors (e.g., TetR and Gal4) and viral activators (e.g., VP16 and VP64) that exhibit robust functionality across many cell types and, in the case of TetR-based systems, are induced by a small-molecule antibiotic (21, 22). However, there are not many of these regulators, thus restricting the number of genes that can be controlled in a circuit. They are also challenging to reprogram for new regulatory relationships, and

their nonmammalian origins and chemical inducers present clinical hurdles for therapies that depend on persistent expression (23, 24). Programmable DNA-targeting elements, such as the bacterial CRISPR-Cas9 system, have provided new methods for gene expression modulation and synthetic circuit design (25–27). However, the large size of Cas9 constrains what can be designed and delivered to primary human cells, and the high immunogenic potential of Cas9 is also well documented (28, 29).

We outlined four basic properties for a toolkit that could support the rapid and scalable construction of gene expression circuits that are effective and potentially suitable for clinical use (Fig. 1A): (i) it should prioritize the use of human-derived proteins, when possible, to minimize immunogenic potential; (ii) it should be orthogonal to minimize cross-talk with native regulation; (iii) there should be safe regulation to ensure gene-regulatory activity that can be easily and safely controlled; and (iv) it should be compact, with minimized genetic footprints for efficient delivery into primary human cells and tissues. As a building block for our toolkit of synthetic regulators, we focused on Cys2His2 zinc fingers (ZFs), which balance clinical favorability and programmability. ZFs are small domains (~30 amino acids) that bind to ~3 base pairs (bp) of DNA (30). They are the most prevalent DNA binding domain found in human transcription factors (31), suggesting that they represent a flexible solution to DNA recognition with low immunogenicity potential. Indeed, a first-generation artificial ZF-based regulatory system showed multiyear functionality in nonhuman primates and had no apparent immunogenicity (32). Moreover, individual ZF domains can be reprogrammed to recognize new motifs and concatenated to generate proteins capable of specifically targeting longer DNA sequences (33–36). Although ZF engineering has been applied to generate endogenous genome editing and manipulation tools, we sought to create a collection of composable synthetic regulators with genome-orthogonal specificities.

We leveraged an archive of engineered two-finger (2F) units that explicitly account for context-dependent effects between adjacent fingers (34, 36). By linking 2F units using flexible “disrupted” linkers (37), it is possible to construct functional 6F arrays capable of recognizing 18 bp, a length for which a random sequence has a high probability of being unique in the human genome (Fig. 1B and fig. S1B). We prioritized 6-bp subsites that are underrepresented in the human genome and selected arrays to minimize identity with the human genome. This yielded 11 targetable synthetic DNA binding motifs (DBMs) (Fig. 1C; fig. S1, C and D; and materials and methods). We next sought to engineer synthetic zinc finger transcription regulators (synZiFTRs) capable of strong

¹Biological Design Center, Boston University, Boston, MA, USA. ²Department of Biomedical Engineering, Boston University, Boston, MA, USA. ³Program in Molecular Biology, Cell Biology, and Biochemistry, Boston University, Boston, MA, USA. ⁴Molecular Pathology Unit, Center for Cancer Research, and Center for Computational and Integrative Biology, Massachusetts General Hospital, Boston, MA, USA. ⁵Department of Pathology, Harvard Medical School, Boston, MA, USA. ⁶Department of Genomics Technologies, Corvea Agriscience, Johnston, IA, USA. ⁷Cell Design Institute and Department of Microbiology and Immunology, University of California, San Francisco, San Francisco, CA, USA. ⁸Parker Institute for Cancer Immunotherapy, University of California, San Francisco, San Francisco, CA, USA. ⁹Helen Diller Family Comprehensive Cancer Center, University of California, San Francisco, San Francisco, CA, USA. ¹⁰Chan Zuckerberg Biohub, San Francisco, CA, USA. ¹¹Wyss Institute for Biologically Inspired Engineering, Harvard University, Boston, MA, USA.

*Corresponding author. Email: khalil@bu.edu (A.S.K.)

†These authors contributed equally to this work.

and specific regulation at these synthetic *cis* elements. We fused ZFs predicted to bind each DBM to the human p65 activation domain and screened for the most active candidates in human embryonic kidney 293FT (HEK293FT) reporter lines (fig. S2, A to C). Selected synZiFTRs strongly activated corresponding, but not non-cognate, reporters (Fig. 1, D and E). To evaluate their impact on native regulation, we performed RNA-sequencing analysis on cell lines expressing three representative synZiFTRs, ZF1, ZF3, and ZF10, benchmarking these against a TetR-based activator. synZiFTR regulation profiles are highly specific, minimally affecting native transcript profiles, and compare favorably with the profile of TetR (Fig. 1F and fig. S3). These results establish a collection of compact, humanized, and genome-orthogonal synZiFTRs optimized for gene expression control and synthetic circuit design in human cells.

To achieve the goal of regulatable synZiFTR circuits, we considered methods for enacting gene regulation control in response to defined input stimuli (Fig. 2A). We focused our attention on user-defined regulation, which in principle allows total control over the timing, level, and context over which a therapeutic gene is expressed. Moreover, regulated circuits with user-defined control over multiple genes could be used to instruct engineered cells to dynamically activate different complementary cellular programs to achieve optimal phenotypes (Fig. 2B). One promising approach for user-defined control is using small molecules, which can be administered systemically or locally to switch ON a gene circuit and/or activate the production of a therapeutic gene product. We prioritized compounds that are already clinically approved or otherwise known to have favorable safety profiles. This resulted in three classes of small molecules that can regulate synZiFTR activity through distinct mechanisms, offering the potential for up to three orthogonal channels of gene expression control (Fig. 2C and fig. S4A). The first is grazoprevir (GZV), a US Food and Drug Administration (FDA)-approved antiviral drug from a family of protease-inhibiting compounds, which has an exceptional safety profile and is commonly taken at a high dose (100 mg/day) for up to 12 weeks (38). The addition of GZV stabilizes synZiFTRs incorporating the NS3 self-cleaving protease domain (from hepatitis C virus), driving gene transcription (39, 40). The second compound is 4-hydroxytamoxifen/tamoxifen (4OHT/TMX), the FDA-approved and widely prescribed breast cancer drug that selectively modulates the nuclear availability of molecules fused to sensitized variants of the human estrogen receptor ERT2 (41, 42). The third compound is abscisic acid (ABA), a plant hormone naturally present in many plant-based foods and classified as non-toxic to humans, which mediates conditional

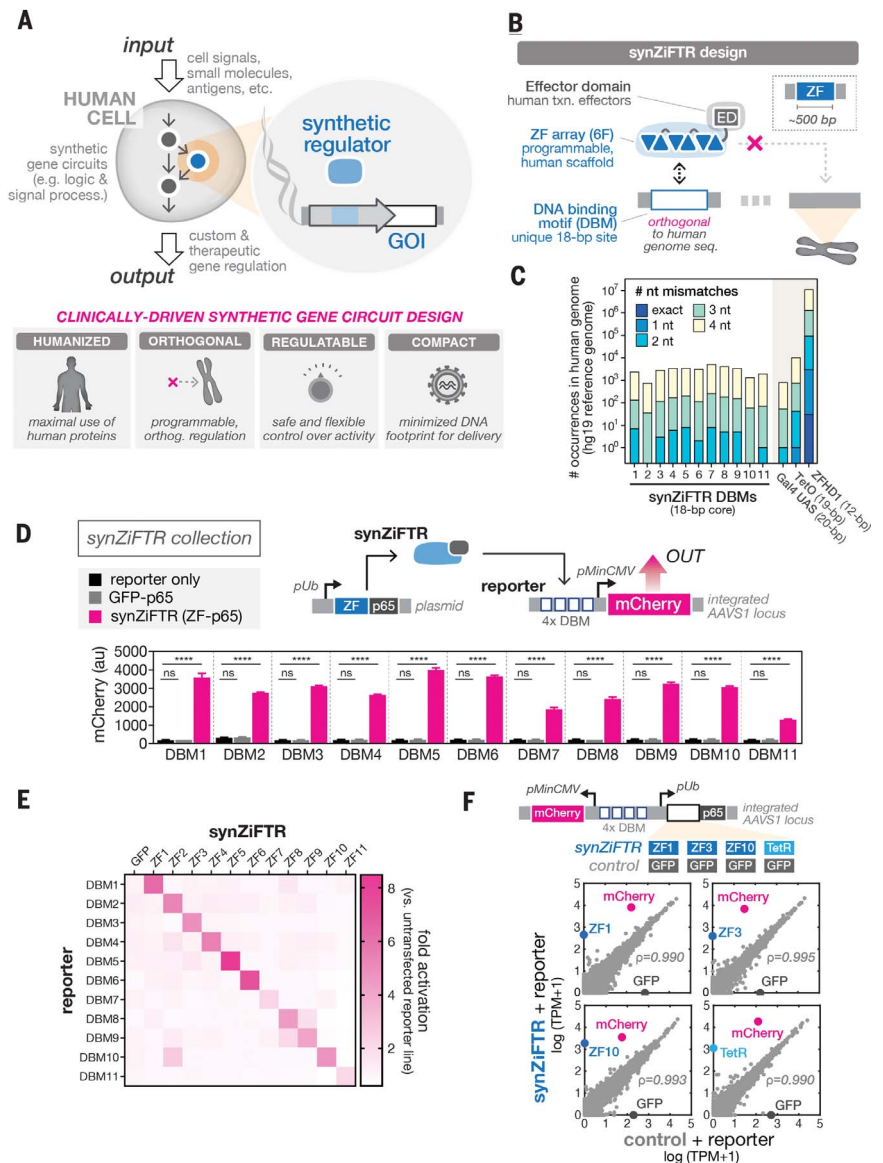


Fig. 1. Clinically driven design of compact, humanized, synthetic gene regulators (synZiFTRs) for mammalian cell engineering. (A) Top: Synthetic gene circuits are used to convert diverse input signals into the desired gene expression outputs to precisely control human cell function. Bottom: Criteria for clinically driven gene circuit design framework. (B) synZiFTR design. synZiFTRs have a modular design that is based on compact, human-derived protein domains. An engineered ZF array mediates interactions with a unique, human genome-orthogonal DBM, and human-derived effector domains (EDs) are used to modulate transcriptional activity. (C) Prevalence of synZiFTR recognition motifs in the human genome. Plotted are the occurrences of exact and increasingly mismatched sequences for each synZiFTR DBM and response elements from common artificial regulators (Gal4 UAS, TetO, and ZFH1). (D) synZiFTRs strongly activate gene expression at corresponding response promoters. Response element vectors were stably integrated into HEK293FT cells to generate reporter lines for each synZiFTR (ZF-p65 fusion). synZiFTR (or control) expression vectors were transfected into corresponding reporter lines, and mCherry was measured by flow cytometry after 2 days. Bars represent mean values for three measurements \pm SD. Statistics represent one-way ANOVA with Dunnett's multiple comparisons; ns, not significant; **** $P < 0.0001$. pUb, ubiquitin C promoter; pMinCMV, minimal CMV promoter; p65, amino acids 361 to 551. (E) synZiFTRs have mutually orthogonal regulatory specificities. Each synZiFTR expression vector was transfected into every reporter line, and mCherry was measured by flow cytometry after 2 days. Fold activation levels represent mean values for three biological replicates. (F) synZiFTRs exhibit specific and orthogonal transcriptional regulation profiles in human cells. Shown is the correlation of transcriptomes from RNA-sequencing measurements of HEK293FT cells stably expressing synZiFTR or TetR-p65 versus a GFP-p65 control. Points represent individual transcript levels normalized to transcripts per kilobase million (TPM), averaged between two technical replicates. The Pearson correlation coefficient was calculated for native (gray) transcripts. See fig. S3 for extended analyses.

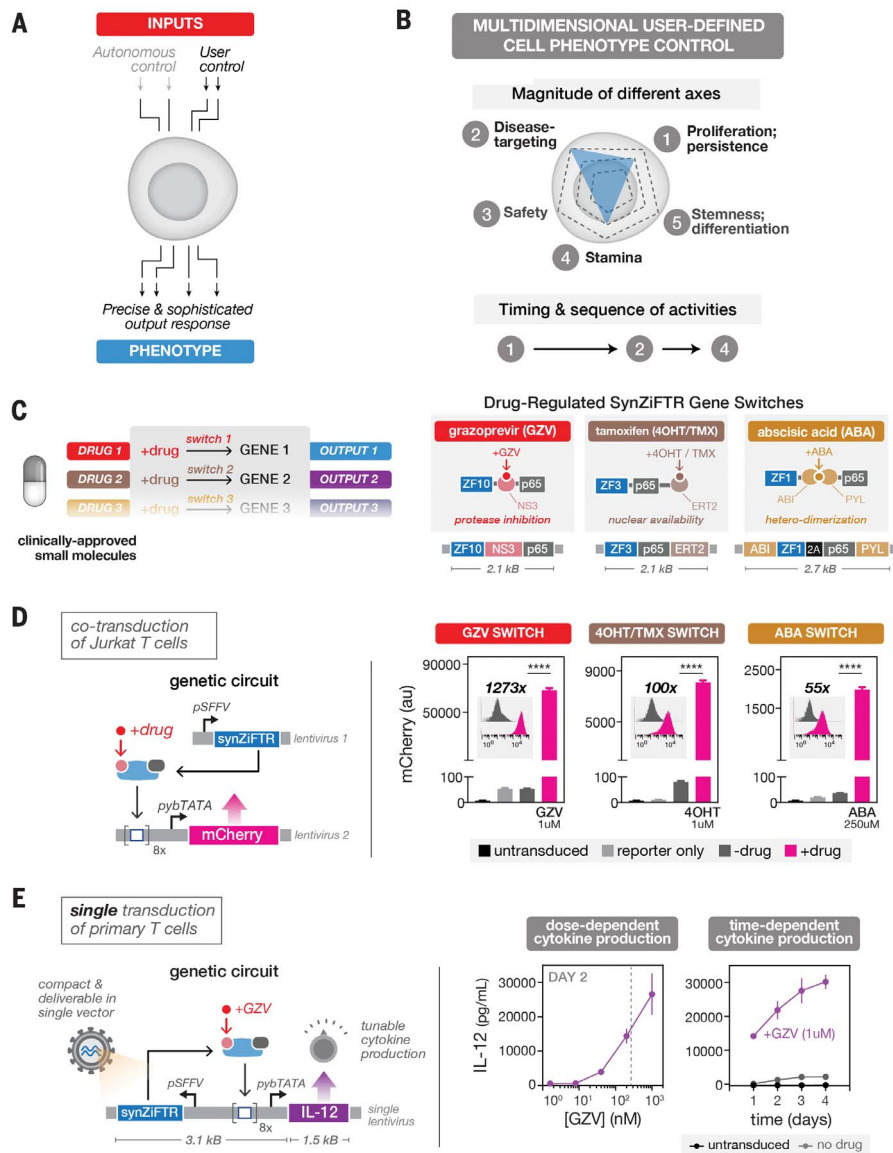


Fig. 2. synZiFTR gene switches allow precise, user-defined control over gene expression in human cells using clinically approved small molecules. (A) Two forms of cellular control: Circuits can be designed to enact cell-autonomous phenotype control (e.g., through recognition of disease-relevant cell surface molecules) or external, user-defined phenotype control (e.g., through administration of small molecules). (B) User-defined control over different axes of a cellular phenotype (top) and the chronology of cellular activities (bottom). (C) Implementing multigene user control with orthogonal gene switches that are regulated by clinically viable small molecules (right). Shown is the design of three distinct synZiFTR gene switches that are controlled by orthogonal small molecules: GZV, 4OHT/TMX, and ABA (right). NS3, hepatitis C virus NS3 protease domain; ERT2, human estrogen receptor T2 mutant domain; ABI, ABA-insensitive 1 domain (amino acids 126 to 423); PYL, PYR1-like 1 domain (amino acids 33 to 209). (D) Optimized synZiFTR switches enable strong inducible gene expression in Jurkat T cells. Jurkat T cells were cotransduced with reporter and synZiFTR expression lentiviral vectors in an equal ratio. mCherry fluorescence was measured by flow cytometry 4 days after induction by small molecules at the indicated concentrations. Bars represent mean values for three measurements \pm SD. Statistics represent two-tailed Student's *t* test; ****P* < 0.001; *****P* < 0.0001. Histograms show absolute levels and mean fold activation for one representative measurement (insets). pSFFV, spleen focus-forming virus promoter; pybTATA, synthetic YB_TATA promoter. (E) Compact, single lentivirus-encoded synZiFTR switches enable titratable control over the expression of therapeutically relevant genes in primary human immune cells. Human primary T cells were transduced with a single lentiviral vector encoding GZV-regulated IL-12 (see the materials and methods). IL-12 production was measured by enzyme-linked immunosorbent assay (ELISA) at specified time points after induction (with or without 1 μ M GZV). Points represent mean values for three measurements \pm SD. Dashed line is the estimate of the C_{max} (maximum serum concentration) for traditional clinical dosing of GZV.

binding of complementary protein fragments (ABI and PYL) from the ABA stress response pathway to reconstitute an active synZiFTR (43). Note that there are trade-offs in priorities. For example, allowing the incorporation of minimal nonhuman-derived domains into the synZiFTR scaffold allows the use of drugs that minimally interfere with native cellular machinery (e.g., GZV) or of inexpensive non-toxic molecules (e.g., ABA).

We constructed GZV-, 4OHT/TMX-, and ABA-inducible gene switches using distinct ZFs (ZF1, ZF3, and ZF10) and tested their performance in Jurkat T cells (fig. S4, A and B). The three systems exhibited titratable control of reporter output, minimal leakage relative to reporter-only cells, strong dynamic ranges, and no cross-reactivity, and they returned to basal levels upon removal of inducer (fig. S4, C and D). Because of the orthogonality of the inducers and the modularity of the synZiFTR architecture, more elaborate gene switches can be readily designed for more complex forms of temporal control, including multiplexed ON/OFF switching (fig. S5).

To optimize synZiFTR circuit dynamics, we screened arrangements of DBM arrays and minimal promoters to identify combinations that reduced basal expression and improved dynamic range (44) (fig. S6A). This produced optimized designs for GZV-, 4OHT-, and ABA-inducible synZiFTR circuits that are encodable in either dual or single lentiviral vectors (Fig. 2D and fig. S6B) and can enable dose- and time-dependent control of therapeutically relevant payloads, such as the immunomodulatory factor interleukin-12 (IL-12), in therapeutically relevant primary human cells (Fig. 2E).

Do synZiFTR circuits enable in vivo, clinically relevant gene expression outputs? To investigate this, we turned to CAR T cell therapy as a proof of principle, initially choosing to develop a gene switch to control CAR expression and activate tumor-targeting functionality (Fig. 3A). This modality allows the rapid evaluation of whether small molecule-dependent synZiFTR activity is sufficient to elicit functional (i.e., disease-modifying) changes in vitro and in vivo, and recent work has established the value of controlling the timing of activation of CAR signaling for improved CAR T cell fitness and outcomes (45–47). We developed a GZV-regulated anti-Her2 CAR (Fig. 3A). Her2 is a receptor tyrosine kinase that is overexpressed in many tumors, including a small subset of leukemias (48). We previously demonstrated this anti-Her2 CAR in a xenograft liquid tumor model, thus providing a convenient platform with which to evaluate the efficacy of our synZiFTR circuits (49). Our gene switch exhibited GZV-dependent CAR expression in primary human T cells at levels comparable to that of a constitutively expressed CAR and

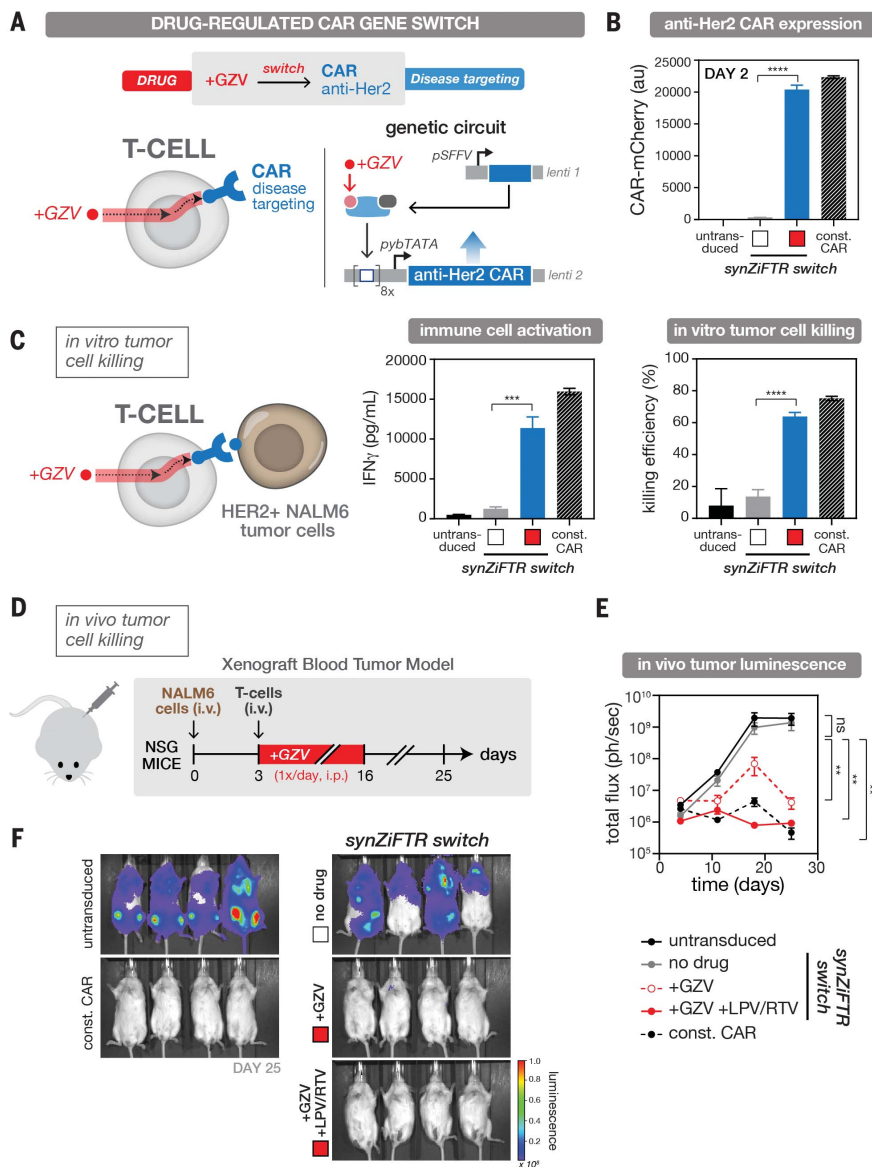


Fig. 3. synZiFTR gene circuit for drug-regulated postdelivery control over CAR expression and T cell killing in vivo. (A) Design of the synZiFTR gene circuit for GZV-dependent control over anti-Her2 CAR expression and tumor cell targeting and killing. (B) GZV-regulated CAR expression in primary T cells. Human primary T cells were co-transduced with equal ratios of lentiviral vectors encoding the synZiFTR CAR gene circuit (see the materials and methods). Expression of anti-Her2 CAR-mCherry was measured by flow cytometry 2 days after induction (with or without 1 μ M GZV). White box, uninduced; red box, GZV induced. Const. CAR, constitutively expressed (pSFFV-CAR). Bars represent mean values for three measurements \pm SD. Statistics represent two-tailed Student's *t* test; *****P* < 0.001; ******P* < 0.0001. (C) GZV-regulated immune cell activation and tumor cell killing in vitro. synZiFTR-controlled CAR T cells (preinduced with or without 1 μ M GZV for 2 days) were cocultured with HER2⁺ NALM6 target leukemia cells in a 1:1 ratio (left). Interferon- γ secretion from activated immune cells was measured by ELISA (center) and tumor cell killing by flow cytometry (right) 1 day after coculturing. White box, uninduced; red box, GZV induced. (D) Testing the in vivo efficacy of synZiFTR-regulated CAR T cells using a xenograft tumor mouse model. Shown is a timeline of an in vivo experiment in which NSG mice were injected intravenously with luciferase-labeled HER2⁺ NALM6 cells to establish tumor xenografts, followed by treatment with T cells. GZV was formulated alone or in combination with LPV/RTV and administered intraperitoneally daily for 14 days. Mice were imaged weekly on days 4, 11, 18, and 25 to monitor tumor growth through luciferase activity. GZV was given at 25 mg/kg and LPV/RTV at 10 mg/kg. (E) Tumor burden over time, quantified as the total flux (photons/second) from the luciferase activity of each mouse using IVIS imaging. Points represent mean values \pm SEM (*n* = 4 mice per condition). Statistics represent two-tailed, ratio-paired Student's *t* test; ns, not significant; ***P* < 0.01. (F) IVIS imaging of mouse groups treated with untransduced cells, synZiFTR-regulated CAR T cells, synZiFTR-regulated CAR T cells with GZV, synZiFTR-regulated CAR T cells with GZV+LPV/RTV, or constitutive CAR cells (*n* = 4 mice per condition).

with minimal output in the absence of inducer (Fig. 3B). When cocultured with Her2-overexpressing (HER2⁺) NALM6 leukemia cells (fig. S7C), synZiFTR-regulated CAR cells were capable of drug-dependent activation and efficient tumor cell killing in vitro (Fig. 3C). These synZiFTR circuits are easily reconfigurable. By swapping the anti-Her2 CAR with an anti-CD19 CAR, we reproduced these in vitro results for a second CAR payload, demonstrating the generalizability of our platform (fig. S7).

Next, we tested the in vivo efficacy of synZiFTR-regulated CAR T cells using a simple xenograft blood tumor model (49) (Fig. 3D and materials and methods). Mice receiving synZiFTR-controlled CAR T cells were treated with GZV either alone or in combination with lopinavir/ritonavir (LPV/RTV), a cocktail known to increase drug bioavailability (50), and were able to clear the tumor. Conversely, those not treated with inducer developed high tumor burdens, as determined by IVIS imaging of luciferase-expressing HER2⁺ tumors (Fig. 3, E and F, and fig. S8, A and B). Although both inducer conditions led to tumor eradication, clearance rates were faster with the cocktail, consistent with the constitutive CAR⁺ control and with the ability of LPV/RTV to increase GZV bioavailability (Fig. 3E and fig. S8C). These results demonstrate that synZiFTR circuits can be used to program drug-dependent, post-delivery control over T cell antitumor activity in vivo.

In addition to controlling CAR-mediated tumor targeting, synZiFTRs are also suited to controlling the expression of other proteins such as IL-2 or IL-12, immunomodulatory cytokines that have long been considered to be potential anticancer agents because of their role in stimulating and regulating immune responses (51, 52). Equipping engineered immune cells to produce cytokines is a compelling approach to improving their antitumor efficacy. However, high doses of IL-2 or IL-12 are known to cause severe side effects. Regulated expression represents a safer approach to leveraging the potential of these factors for augmenting immune cell efficacy. Moreover, as a T cell growth factor, user-regulated IL-2 production could serve as an exciting basis for achieving on-demand cellular proliferation.

To establish a proliferation gene switch, we used a TMX-inducible synZiFTR to regulate the expression of super IL-2, an enhanced version of IL-2 with stronger affinity to CD122 (53) (Fig. 4A). Our gene switch exhibited 4OHT/TMX-dependent super IL-2 production in vitro in primary T cells, once again to levels comparable to that of the constitutive control and with minimal output in the absence of inducer (Fig. 4B). Primary T cells require exogenous IL-2 to remain viable over long periods of time

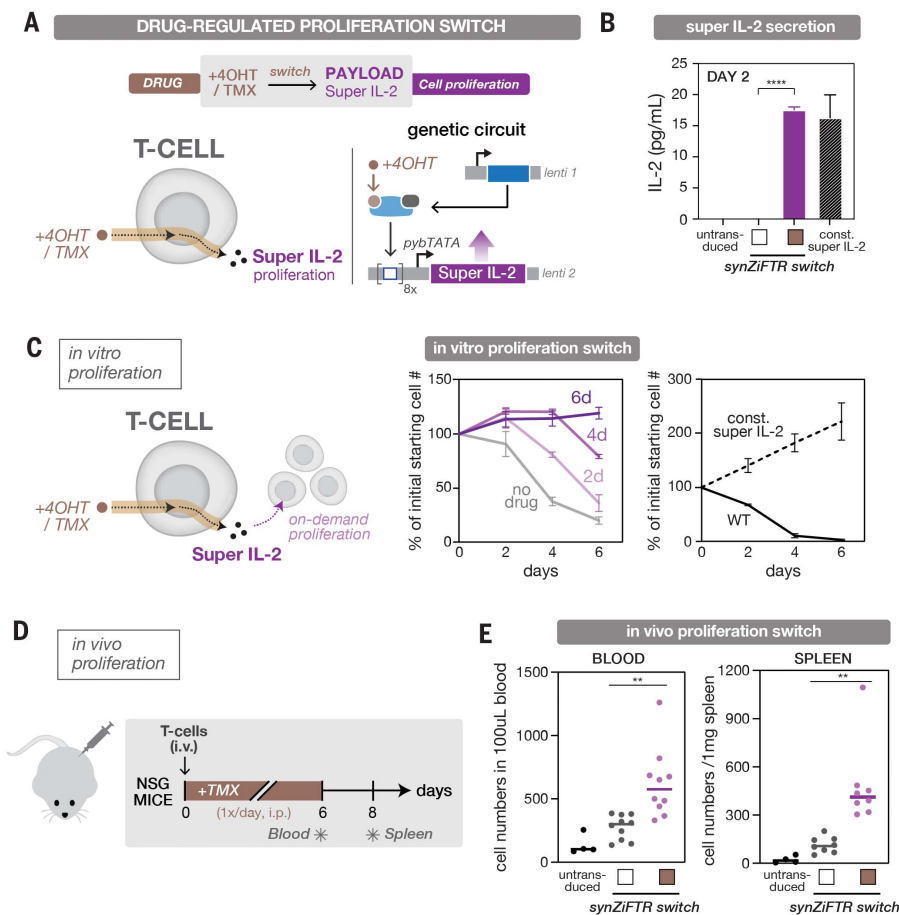


Fig. 4. synZiFTR gene circuit for drug-regulated, on-demand immune cell proliferation. (A) Design of the synZiFTR gene circuit for 4OHT/TMX-dependent control over super IL-2 expression and cell proliferation. (B) 4OHT-regulated super IL-2 production in primary T cells. Human primary T cells were cotransduced with equal ratios of lentiviral vectors encoding the synZiFTR-regulated proliferation gene circuit (see the materials and methods). Secretion of super IL-2 was measured by ELISA (for IL-2) 2 days after induction (with or without 1 μ M 4OHT). White box, uninduced; brown box, 4OHT induced. Const. super IL-2, constitutively expressed (pSFV-super IL-2). Bars represent mean values for three measurements \pm SD. Statistics represent two-tailed Student's *t* test; ****P* < 0.001; *****P* < 0.0001. (C) 4OHT-regulated T cell proliferation in vitro. synZiFTR-regulated primary T cells were cultured in IL-2-free media, induced with 4OHT (1 μ M) for different durations, and live-cell numbers were quantified by flow cytometry at the indicated days (center). Untransduced (wild-type) and constitutively expressing (const. super IL-2) T cells were cultured and quantified similarly (right). Lines represent mean values for three measurements \pm SD. (D) Testing the in vivo efficacy of the drug-regulated, on-demand proliferation switch. Shown is a timeline of an in vivo experiment in which NSG mice were injected intravenously with primary T cells followed by daily treatment with TMX over 6 days. The blood and spleen were individually sampled on days 6 and 8, respectively, to quantify the change in T cell numbers. TMX was given at 75 mg/kg. (E) TMX-regulated T cell expansion in vivo. Human T cell numbers from blood and spleen samples were quantified by flow cytometry by gating for hCD3⁺/mCD45⁻ cells after staining for human CD3 (hCD3) and mouse CD45 (mCD45). Lines indicate the mean value; dots represent each mouse. Blood sample, *n* = 10; spleen sample, *n* = 8. White box, uninduced; brown box, TMX induced. Statistics represent two-tailed Student's *t* test; ***P* < 0.01.

in culture, which provides a simple way to test the performance of the proliferation switch. We cultured equal numbers of engineered cells in media lacking IL-2 and induced them with 4OHT for different durations. Cells harboring the inducible super IL-2 switch exhibited duration-dependent proliferation (Fig.

4C). The synthetic system also exhibited dose-dependent control over super IL-2 production and cellular proliferation (fig. S9). Finally, to demonstrate the ability of the proliferation switch to control T cell growth in vivo, we injected engineered T cells into NSG mice intravenously and administered TMX

daily through intraperitoneal injection for 6 days. We observed enhanced T cell levels in the peripheral blood (day 6) and spleen (day 8) in mice receiving engineered T cells and exposed to TMX compared with mice receiving engineered T cells without TMX or untransduced cells only (Fig. 4, D and E). These results establish a synZiFTR gene switch for TMX-dependent control over super IL-2 production and in vivo, on-demand cell expansion.

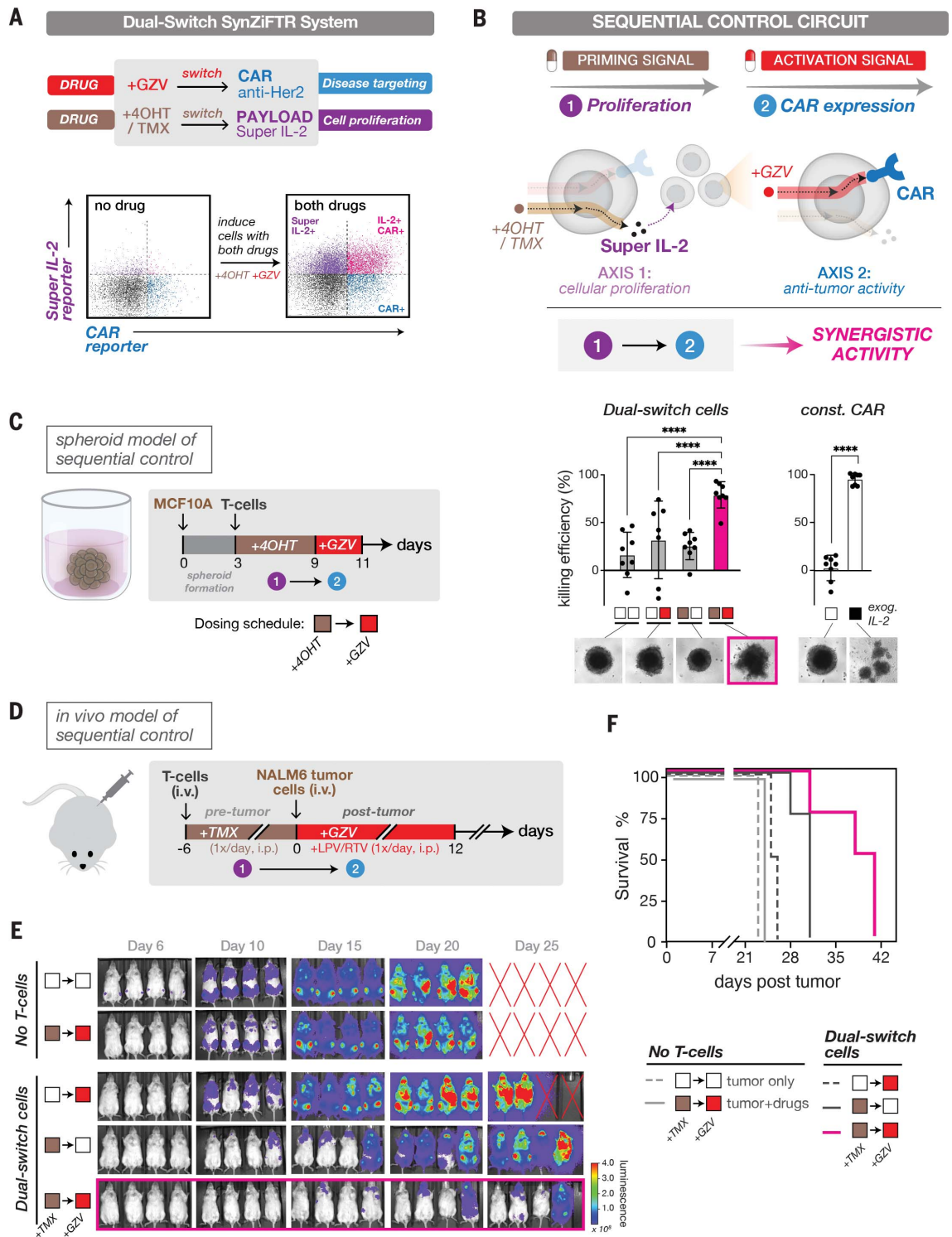
The synZiFTR platform therefore enables the development of compact gene switches that are effective for dose- and time-dependent control of therapeutically relevant genes both in vitro and in vivo, setting the stage for genetic circuits that allow simultaneous and independent multigene control in the same cell. To investigate whether synZiFTRs can regulate two orthogonal gene programs, we transduced primary human T cells with vectors encoding GZV-regulated anti-Her2 CAR and TMX-regulated super IL-2 switches (Fig. 5A). Next, we induced cells with different combinations of the two drugs and used distinguishable reporters to measure gene activation for each channel. Engineered cells exhibited the desired orthogonal patterns of gene activation (fig. S10A). After induction with both drugs, >14% of cells simultaneously expressed high levels of both genes (Fig. 5A). Thus, our full dual-switch genetic circuit was delivered to a significant population of cells, and both switches were functional and orthogonal.

A capability afforded by dual-switch circuits is the possibility of enacting sequential control of cell function (Fig. 5B). Modulating cell functions on the basis of the timing and sequential order of signaling events is a critical regulatory mechanism in living systems (54, 55), including in the immune system (56). Motivated by natural systems, engineered sequential control could dictate when and in what order distinct cellular programs are activated, potentially unlocking underexplored dimensions of cell therapy function. As a proof of principle, we envisioned a simple scenario in which a small starting population of engineered cells is first "primed" with one signal (4OHT/TMX, to drive cellular expansion and poise cells for activation) and subsequently "activated" by a second signal (GZV, to induce CAR expression and initiate antitumor activity) (Fig. 5B). We then set out to develop models to determine whether we could establish sequential control of immune cells in vitro and in vivo.

We began with a two-dimensional (2D) in vitro model that builds upon the cell proliferation experiments shown in Fig. 4. We cultured synZiFTR-controlled T cells for 6 days either with or without the priming signal (4OHT), activated CAR expression (with

Fig. 5. Enacting sequential control of immune cell function to drive synergistic in vivo responses.

(A) Dual-switch synZiFTR system for orthogonal, drug-inducible control over anti-Her2 CAR and super IL-2 expression (top). Circuit activation in primary T cells was assessed after induction with both drugs (1 μ M GZV and 1 μ M 4OHT) (bottom). Distinguishable reporters were used to measure gene activation for each channel with or without 1 day of induction: mCherry-fused anti-Her2 CAR and bicistronic super IL-2 reporter (super IL-2-2A-EGFP). See also fig. S10. (B) Schema for sequential control in which a priming signal (4OHT/TMX drug) was used to induce cellular proliferation of a small starting population of dual-switch cells through super IL-2 expression, followed by an activation signal (GZV) to induce cytotoxic activation through CAR expression. (C) In vitro spheroid model used to demonstrate the synergistic efficacy of sequential control over T cell proliferation (+4OHT) and activation (+GZV) behavior (left). T cell killing efficiency was measured by luminescence signals from spheroids, and representative morphology of spheroids at the end point is shown below (right). White box, uninduced; brown box, 4OHT induced; red box, GZV induced. Bars represent mean values \pm SD. Const. CAR, constitutive CAR cells. (D) An in vivo model used to demonstrate the synergistic efficacy of sequential control over T cell proliferation (+TMX) and activation (+GZV) behavior. Shown is a timeline of an in vivo experiment in which NSG mice were injected intravenously with dual-switch T cells (1×10^6 cells) 6 days before the tumor challenge. TMX was administered intraperitoneally daily over 6 days to activate the proliferation switch before tumor challenge. HER2⁺/Luciferase⁺ NALM6 cells (1×10^6 cells) were injected intravenously 6 days after injection of T cells, and the GZV-regulated CAR was switched ON by administering GZV in combination with LPV/RTV daily intraperitoneally over 12 days. TMX was given at 75 mg/kg, GZV at 25 mg/kg, and LPV/RTV at 10 mg/kg. (E) IVIS imaging of tumor burden over time of mouse groups treated with tumor alone (no T cells), tumor with both drugs in sequence (TMX \rightarrow GZV), dual-switch T cells treated with GZV alone during the time window of day 0 \rightarrow day 12 ($\emptyset \rightarrow$ GZV), dual-switch T cells treated with TMX alone during the time window of day 6 \rightarrow day 0 (TMX $\rightarrow \emptyset$), and dual-switch T cells treated with both drugs in sequence (TMX \rightarrow GZV). (F) Kaplan-Meier survival curves for the various treatment groups for the in vivo sequential model study ($n = 4$ mice per condition). White box, uninduced; brown box, TMX induced; red box, GZV induced.



GZV), and subsequently challenged with HER2⁺ NALM6 tumor cells 1 day after activation, comparing these cells with constitutive CAR-expressing cells (fig. S10B). Only cells harboring the dual-switch circuit exhibited expansion of cell numbers when induced with 4OHT (fig. S10C). Correspondingly, we found that only dual-switch cells that were 4OHT primed and subsequently GZV activated (4OHT → GZV) were capable of efficient tumor cell killing when challenged with fast-growing tumor cells 1 week (day 7) after initiating the culture (fig. S10D). Encouraged by these results, we sought to establish a 3D spheroid model of sequential control (Fig. 5C). Spheroids are an imperfect but useful model of in vivo solid tumors, sharing notable morphological and behavioral similarities, including the development of oxygen and nutrient gradients, the formation of a necrotic/apoptotic central core, and recapitulation of 3D cell-cell and cell-matrix interactions (57). We designed a 3D spheroid based on HER2⁺ MCF10A breast mammary epithelial cells, which we used to test whether sequential control can drive functional changes to the spheroid targets (Fig. 5C and materials and methods). Spheroids cocultured with dual-switch cells and receiving the sequential 4OHT → GZV dose regimen exhibited synergistic responses, as measured by tumor cell killing and the corresponding morphological disruption of spheroids, including loss of their hallmark rounded shape and amorphous cell scattering throughout the well (Fig. 5C). These results provide evidence for engineered sequential control of T cell function in vitro.

Our next goal was to develop an in vivo model of sequential control. To look for conditions in which we could evaluate the control circuit, we modulated the infusion timing of constitutive CAR T cells in an NSG mouse leukemia model. Mice received either a preinfusion (at day -6) or a postinfusion (day 1) of a relatively low number of control constitutive CAR-expressing T cells (1×10^6 cells) (fig. S11A). At day 0, we injected the mice with HER2⁺ Nalm6 tumor cells and tracked tumor burden. The preinfused CAR T cells were less effective at responding to the tumor challenge (fig. S11, B and C). The 6-day preinfusion tumor model offers a window of susceptibility to demonstrate the sequential control circuit. When we tested dual-switch T cells in this mouse model (Fig. 5D), we observed synergistic in vivo activity in reducing tumor burden in mice receiving the engineered T cells and the TMX → GZV dose regimen relative to other dosing schemes and non-T cell controls (Fig. 5, E and F, and fig. S11D). Mice that were not preconditioned with the TMX stimulus before the tumor cell challenge but were induced to activate CAR expression were significantly less effective at responding to the challenge, sug-

gesting that the TMX phase was necessary for priming the population. These results provide evidence that we can engineer sequential control of T cell function in vivo using orthogonal FDA-approved drugs as stimuli. They also demonstrate the therapeutic potential of these circuits that can sequentially activate therapeutically relevant and synergistic genes to prime cells for antitumor activity.

In this work, we designed and tested in human cells a suite of clinically inspired synthetic gene regulators and circuits with demonstrated therapeutic potential. The synZiFTR platform features de novo-engineered ZFs that can be used to implement orthogonal and clinically viable drug-controlled genetic circuits with minimal genetic footprints. Using this platform, we demonstrated new capabilities for user-defined control over therapeutic cell function, including the creation of multi-input/-output circuits that enable sequential control of immune cell function to drive synergistic in vivo activity in reducing tumor burden.

We undertook the design of ZFs because of their hypercompact size, human origin, and demonstrated clinical viability. Moreover, we and others have demonstrated that ZF systems permit tunability at the level of DNA binding affinity and cooperativity, which is valuable in designing synthetic circuits with tunable and predictive input/output behaviors (58–60). Other programmable DNA-targeting systems use large proteins of nonhuman origin, which may pose issues with regard to immunogenicity. Analysis of our core synZiFTR architecture using an established immunogenicity prediction tool confirmed that our ZF peptides have lower predicted immunogenicity scores compared with those of TetR, Gal4, and *sp* dCas9 (fig. S12 and materials and methods). However, evaluating the true immunogenic potential of any synthetic system will ultimately require empirical measurements. Although the initial synZiFTR platform is based upon ZFs, alternative methods of gene activation, such as CRISPR-Cas systems engineered to have reduced size and immunogenic potential (61–63), may in the future complement the platform.

We outlined criteria to guide clinically driven gene circuit design processes. As we demonstrated with our gene switches, developing systems within this framework is a multidimensional optimization problem that will require prioritizing specific criteria depending on the application. Our GZV switch favors safe regulation, prioritizing the use of a clinically approved, pharmacokinetically favorable drug that does not target native cellular proteins. The TMX switch offers an entirely human-derived option. Overall, we believe that our synZiFTR systems offer superior options to existing drug-regulated systems because of the

combination of drug safety, efficacy, regulatory orthogonality, and predicted low immunogenicity. In the future, efforts to predict potential immunogenic peptides (fig. S12), “de-immunize” synZiFTR domains, and perhaps incorporate new human-derived ligand-binding domains with biocompatible inducers could provide pathways to clinical translation. Finally, because of the modularity and orthogonality of the synZiFTR architecture, it should be relatively straightforward to incorporate other regulatory domains, including de novo-designed bioactive protein domains (64, 65), and to use synZiFTRs as the basis for constructing cell-autonomous and multi-antigen recognition circuits (11, 12, 66).

The ability to encode temporal patterns using synZiFTR sequential control circuits could unlock an underexplored dimension of cell therapy function. For instance, the type 2 effector response is typically viewed as protumor; however, evidence is accumulating that it can also mediate antitumor immunity (67, 68). One possible way to harness the type 2 response could be to activate it after an initial cytotoxic response by CAR T cells. Our synZiFTR platform would be ideally suited to perform such a complex therapeutic program safely and effectively.

We expect that our synZiFTR platform will translate widely to other clinically relevant cell types and contexts, enabling the future development of synthetic circuits for gene and cell therapies. Much more development remains and there are many other clinical considerations to address, but we hope these tools will begin to transform the rapid advances we are witnessing in mammalian synthetic biology into new solutions for safer, effective, and more powerful next-generation therapies.

REFERENCES AND NOTES

- M. A. Fischbach, J. A. Bluestone, W. A. Lim, *Sci. Transl. Med.* **5**, 179ps7 (2013).
- T. Kitada, B. DiAndreth, B. Teague, R. Weiss, *Science* **359**, eaad1067 (2018).
- M. Xie, M. Fussenegger, *Nat. Rev. Mol. Cell Biol.* **19**, 507–525 (2018).
- W. A. Lim, C. H. June, *Cell* **168**, 724–740 (2017).
- K. A. Hay, *Br. J. Haematol.* **183**, 364–374 (2018).
- R. A. Morgan et al., *Mol. Ther.* **18**, 843–851 (2010).
- G. Fucà, L. Reppel, E. Landoni, B. Savoldo, G. Dotti, *Clin. Cancer Res.* **26**, 2444–2451 (2020).
- S. Rafiq, C. S. Hackett, R. J. Brentjens, *Nat. Rev. Clin. Oncol.* **17**, 147–167 (2020).
- L. Zhang et al., *Clin. Cancer Res.* **21**, 2278–2288 (2015).
- X. J. Gao, L. S. Chong, M. S. Kim, M. B. Elowitz, *Science* **361**, 1252–1258 (2018).
- K. T. Roybal et al., *Cell* **164**, 770–779 (2016).
- K. T. Roybal et al., *Cell* **167**, 419–432.e16 (2016).
- L. Schukur, B. Geering, G. Charpin-El Hamri, M. Fussenegger, *Sci. Transl. Med.* **7**, 318ra201 (2015).
- M. Xie et al., *Science* **354**, 1296–1301 (2016).
- B. D. Choi et al., *Nat. Biotechnol.* **37**, 1049–1058 (2019).
- V. Golumba-Nagy, J. Kuehle, A. A. Hombach, H. Abken, *Mol. Ther.* **26**, 2218–2230 (2018).
- B. Hu et al., *Cell Rep.* **20**, 3025–3033 (2017).

18. E. Lanitis, G. Coukos, M. Irving, *Curr. Opin. Biotechnol.* **65**, 75–87 (2020).
19. S. Mardiana, B. J. Solomon, P. K. Darcy, P. A. Beavis, *Sci. Transl. Med.* **11**, eaaw2293 (2019).
20. M. Hong, J. D. Clubb, Y. Y. Chen, *Cancer Cell* **38**, 473–488 (2020).
21. S. Braselmann, P. Graninger, M. Busslinger, *Proc. Natl. Acad. Sci. U.S.A.* **90**, 1657–1661 (1993).
22. M. Gossen, H. Bujard, *Proc. Natl. Acad. Sci. U.S.A.* **89**, 5547–5551 (1992).
23. D. Favre et al., *J. Virol.* **76**, 11605–11611 (2002).
24. A. M. Lena, P. Giannetti, E. Sporeno, G. Ciliberto, R. Savino, *J. Gene Med.* **7**, 1086–1096 (2005).
25. L. A. Gilbert et al., *Cell* **154**, 442–451 (2013).
26. P. Perez-Pinera et al., *Nat. Methods* **10**, 973–976 (2013).
27. J. G. Zalatan et al., *Cell* **160**, 339–350 (2015).
28. C. T. Charlesworth et al., *Nat. Med.* **25**, 249–254 (2019).
29. D. L. Wagner et al., *Nat. Med.* **25**, 242–248 (2019).
30. N. P. Pavletich, C. O. Pabo, *Science* **252**, 809–817 (1991).
31. S. A. Lambert et al., *Cell* **175**, 598–599 (2018).
32. V. M. Rivera et al., *Blood* **105**, 1424–1430 (2005).
33. R. R. Beerli, C. F. Barbas3rd, *Nat. Biotechnol.* **20**, 135–141 (2002).
34. M. L. Maeder, S. Thibodeau-Beganny, J. D. Sander, D. F. Voytas, J. K. Joung, *Nat. Protoc.* **4**, 1471–1501 (2009).
35. C. O. Pabo, E. Peisach, R. A. Grant, *Annu. Rev. Biochem.* **70**, 313–340 (2001).
36. J. D. Sander et al., *Nat. Methods* **8**, 67–69 (2011).
37. M. Moore, A. Klug, Y. Choo, *Proc. Natl. Acad. Sci. U.S.A.* **98**, 1437–1441 (2001).
38. J. K. Rockstroh et al., *Lancet HIV* **2**, e319–e327 (2015).
39. C. L. Jacobs, R. K. Badiee, M. Z. Lin, *Nat. Methods* **15**, 523–526 (2018).
40. E. P. Tague, H. L. Dotson, S. N. Tunney, D. C. Sloas, J. T. Ngo, *Nat. Methods* **15**, 519–522 (2018).
41. R. Feil et al., *Proc. Natl. Acad. Sci. U.S.A.* **93**, 10887–10890 (1996).
42. A. K. Indra et al., *Nucleic Acids Res.* **27**, 4324–4327 (1999).
43. F. S. Liang, W. Q. Ho, G. R. Crabtree, *Sci. Signal.* **4**, rs2 (2011).
44. C. Ede, X. Chen, M. Y. Lin, Y. Y. Chen, *ACS Synth. Biol.* **5**, 395–404 (2016).
45. J. H. Choe et al., *Sci. Transl. Med.* **13**, eabe7378 (2021).
46. A. Hyrenius-Wittsten et al., *Sci. Transl. Med.* **13**, eabd8836 (2021).
47. E. W. Weber et al., *Science* **372**, eaba1786 (2021).
48. P. Chevallier et al., *Haematologica* **89**, 1399–1401 (2004).
49. J. H. Cho, J. J. Collins, W. W. Wong, *Cell* **173**, 1426–1438.e11 (2018).
50. H. P. Feng et al., *Antimicrob. Agents Chemother.* **63**, e02142-18 (2019).
51. J. Cohen, *Science* **270**, 908 (1995).
52. J. P. Leonard et al., *Blood* **90**, 2541–2548 (1997).
53. A. M. Levin et al., *Nature* **484**, 529–533 (2012).
54. J. E. Purvis et al., *Science* **336**, 1440–1444 (2012).
55. L. Cai, C. K. Dalal, M. B. Elowitz, *Nature* **455**, 485–490 (2008).
56. G. Napolitani, A. Rinaldi, F. Bertoni, F. Sallusto, A. Lanzavecchia, *Nat. Immunol.* **6**, 769–776 (2005).
57. F. Mittler et al., *Front. Oncol.* **7**, 293 (2017).
58. C. J. Bashor et al., *Science* **364**, 593–597 (2019).
59. P. S. Donahue et al., *Nat. Commun.* **11**, 779 (2020).
60. A. S. Khalil et al., *Cell* **150**, 647–658 (2012).
61. F. A. Ran et al., *Nature* **520**, 186–191 (2015).
62. P. Pausch et al., *Science* **369**, 333–337 (2020).
63. X. Xu et al., *Mol. Cell* **81**, 4333–4345.e4 (2021).
64. R. A. Langan et al., *Nature* **572**, 205–210 (2019).
65. Z. Chen et al., *Nature* **565**, 106–111 (2019).
66. I. Zhu et al., *Cell* **185**, 1431–1443.e16 (2022).
67. M. Liu et al., *Nature* **587**, 115–120 (2020).
68. Z. Bai et al., *Sci. Adv.* **8**, eabj2820 (2022).
69. Data for: H.-S. Li, D. V. Israni, K. A. Gagnon, K. A. Gan, M. H. Raymond, J. D. Sander, K. T. Roybal, J. K. Joung, W. W. Wong, A. S. Khalil, Multidimensional control of therapeutic human cell function with synthetic gene circuits, *Dryad* (2022); <https://doi.org/10.5061/dryad.s7h44j19v>.
70. Code for: H.-S. Li, D. V. Israni, K. A. Gagnon, K. A. Gan, M. H. Raymond, J. D. Sander, K. T. Roybal, J. K. Joung, W. W. Wong, A. S. Khalil, Multidimensional control of therapeutic human cell function with synthetic gene circuits, *Zenodo* (2022); <https://doi.org/10.5281/zenodo.7216675>.

ACKNOWLEDGMENTS

We thank M. Bobbin for technical assistance with the design of ZF arrays and C. Bashor, J. Ngo, and members of the Wong and Khalil laboratories for helpful discussions. **Funding:** This work was supported by the National Institutes of Health (NIH) (grant RO1EB029483 to K.T.R., W.W.W., and A.S.K. and grant DP1 OD006862 to J.K.J.) and the National Science Foundation (NSF) (grant MCB-1713855 to A.S.K.). D.V.I. was supported by a NSF Graduate Research Fellowship (DGE-1247312). A.S.K. was supported by a DARPA Young Faculty Award (D16AP00142), an NIH Director's New Innovator Award (DP2AI131083), and a Department of Defense Vannevar Bush Faculty Fellowship (N00014-20-1-2825). **Author contributions:** D.V.I., J.D.S., and J.K.J. designed ZF proteins and target sequences. D.V.I. performed bioinformatic and sequencing analyses. D.V.I. designed genetic constructs and performed experiments related to Fig. 1. H.-S.L. and D.V.I. designed genetic constructs and performed experiments related to Fig. 2. H.-S.L. designed genetic constructs and

performed experiments related to Figs. 3 to 5. K. A. Gagnon developed the 3D tumor spheroid model and performed spheroid experiments with H.-S.L. K. A. Gan and M.H.R. assisted with developing and testing genetic constructs for the dual-switch system. K.T.R., W.W.W., and A.S.K. oversaw the study. All authors analyzed the data. H.-S.L., D.V.I., M.H.R., W.W.W., and A.S.K. wrote the manuscript with input from all authors. **Competing interests:** D.V.I., J.D.S., J.K.J., and A.S.K. are inventors on a patent related to the synZiFTR technology. H.-S.L., D.V.I., K.T.R., W.W.W., and A.S.K. have filed patent applications related to drug-regulated synZiFTRs. J.K.J. is a coinventor on various patents and patent applications that describe gene editing and epigenetic editing technologies. K.T.R. is a cofounder of Arsenal Biosciences, was a founding scientist/consultant and stockholder in Cell Design Labs, now a Gilead Company, and holds stock in Gilead. J.K.J. has, or had during the course of this research, financial interests in several companies developing gene editing technology: Beam Therapeutics, Blink Therapeutics, Chroma Medicine, Editas Medicine, EpiLogic Therapeutics, Excelsior Genomics, Hera Biolabs, Monitor Biotechnologies, Nvelop Therapeutics (f/k/a ETx, Inc.), Pairwise Plants, Poseida Therapeutics, SeQure Dx, Inc., and Verve Therapeutics. J.K.J.'s financial interests in these companies include consulting fees and/or equity. J.K.J.'s interests were reviewed and are managed by Massachusetts General Hospital and Mass General Brigham in accordance with their conflict of interest policies. W.W.W. is a scientific cofounder of and holds equity in Senti Biosciences. A.S.K. is a scientific adviser for and holds equity in Senti Biosciences and Chroma Medicine and is a cofounder of Fynch Biosciences and K2 Biotechnologies. The remaining authors declare no competing interests. **Data and materials availability:** Plasmids encoding select synZiFTR constructs have been deposited at Addgene for distribution. All DNA constructs and cell lines are available from A.S.K. All sequencing data have been deposited in the Sequence Read Archive (SRA) under the BioProject accession code PRJNA714135. All other datasets have been deposited on Dryad (69). Computer code is available at <https://github.com/khalilab/synZiFTR-analyses> and is archived on Zenodo (70). **License information:** Copyright © 2022 the authors, some rights reserved; exclusive licensee American Association for the Advancement of Science. No claim to original US government works. <https://www.science.org/about/science-licenses-journal-article-reuse>

SUPPLEMENTARY MATERIALS

science.org/doi/10.1126/science.ade0156

Materials and Methods

Figs. S1 to S12

Tables S1 to S3

References (71–81)

MDAR Reproducibility Checklist

[View/request a protocol for this paper from Bio-protocol.](#)

Submitted 19 July 2022; accepted 25 October 2022

10.1126/science.ade0156